12

Pulse energy of a non-relativistic, high-current electron beam

© *P.P. Kiziridi, G.E. Ozur*

Institute of High Current Electronics, Siberian Branch, Russian Academy of Sciences, Tomsk, Russia
e-mail: kiziridi_pavel@mail.ru

Energetic characteristics of a high-current electron gun with a cathode assembly based on multi-gap initiation of explosive emission by dielectric surface flashover in the mode of vacuum and gas-filled diode were investigated. It has been shown that it is better to measure high-current electron beam pulse energy using a calorimetric (thermal imaging) method than to calculate it from the waveforms of accelerating voltage and beam current onto collector (target) since the beam current values may be essentially overstated because of decay current of a dense plasma emergent under the bombardment of a collector by the beam electrons. The best efficiency of the energy transfer from the capacitive storage of the high-voltage pulsed generator supplying an electron gun was observed in the case of gas-filled diode at a moderate pressure of the working gas (argon, 0.093 Pa).

Keywords: high-current electron beams, explosive emission, multi-gap initiation, dielectric surface flashover, beam pulse energy, plasma decay current, thermal imaging.

Introduction

The pulse beam energy and the efficiency of transmission of energy accumulated in the primary storage (usually a capacitive one) into the beam energy are the important characteristics of any source of the accelerated electrons. It is fully related to sources of nonrelativistic $(10-30 \, \text{keV})$ high-current (up to 25 kA) electron beams (NHEB) of a microsecond duration which are widely used for modification of the surface layers of the metal materials [1–8]. Previously, these beams were generated usually in guns with a plasma anode and a multi-wire explosive emission cathode, whose emitting part was made of a radio-frequency cable copper braid [8]. In 2020, we had developed and successfully tested a new cathode assembly with multi-gap initiation of the explosive emission by the dielectric surface flashover [9,10]. The emission characteristics of this cathode assembly have been investigated to show that its average current density in $1.5-2.3$ times exceeds a similar value, which is typical for the traditional gun with the plasma anode and the multi-wire explosive emission copper cathode [10]. Besides, the range of accelerating voltages was extended towards the low values: from 15 to 5 kV, due to the fact that the breakdown voltages along the dielectric are substantially lower than at the vacuum breakdown without it. It is very important for surface modification of the materials which require a moderate value of the energy density $(1-2 \, \text{J/cm}^2)$, for example, surface alloys Ti−Ta at the NiTi substrate [1,2]. The important advantage of the new cathode assembly also includes NHEB generability without the plasma anode, i.e. in the vacuum or gas-filled diode. The present paper continuing the papers [9,10] investigates the energy characteristics of the high-current electron gun with this cathode assembly.

1. Experimental procedure

The experiments have used the electron-beam facility (the electron energy up to 30 keV, the beam current up to 30 kA, the current density up to $1.5 \, \text{kA/cm}^2$, the pulse duration of $2-4 \, \mu\text{s}$), whose design and operating principle are described in the papers [9,10]. The multi-gap initiation of explosive electron emission was performed by means of 69 resistively decoupled arc plasma sources, whose electrodes and tubular ceramic insulators are built into the cathode disc copper substrate. The area of the cathodes emitting part was $19.6 \, \text{cm}^2$. As in [9,10], the capacitance of the high-voltage pulse generator (HVPG) was $C = 2.87 \, \mu\text{F}$. The pressure of the residual gases within the gun volume did not exceed $10^{-2} \, \text{Pa}$.

The accelerating voltage pulses were recorded by the resistive divider, so were the cathode current and the collector beam current — by the Rogowsky coil. Some experiments included measurement of the current beam using a low-inductive shunt with a resistance of 0.005 or $0.02 \, \Omega$. The signals from the sensors were fed to the inputs of a 4-channel broadband (200 MHz) digital oscilloscope Tektronix TDS 2024. It should be noted immediately that the obtained waveforms were identical independently of a source designed to measure the collector beam current.

The beam energy was determined by two methods. The first method included integration of waveforms of pulses of the accelerating voltage and the collector beam current. At the same time, the waveform of the accelerating voltage was adjusted taking into account voltage drops at the inductances in the circuit of the cathode (from a location of the voltage sensor to the cathode) and the collector (anode). The second method is based on processing the thermograms (Fig. 1, *a, b*) obtained using the thermal imager TESTO-875-
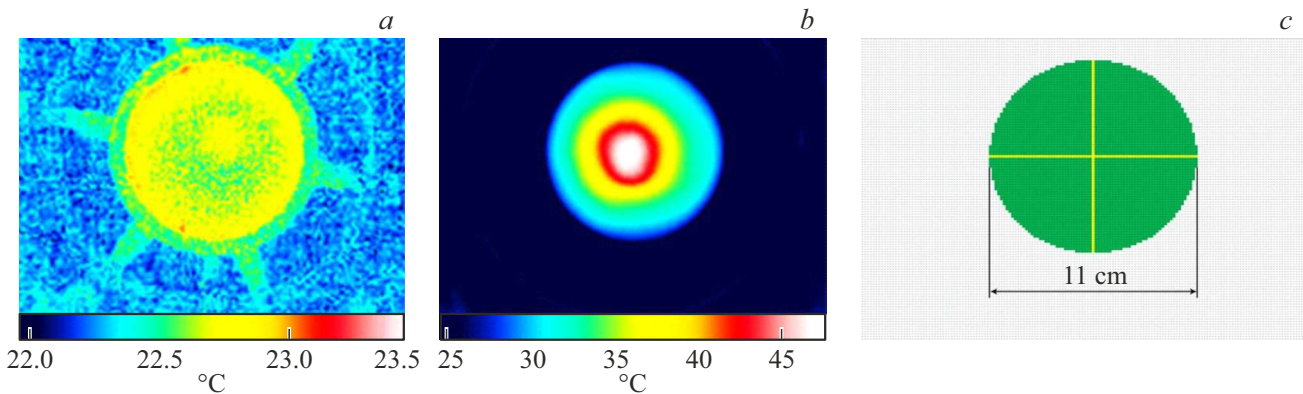
Figure 1. *a* — the background thermogram, *b* — the thermogram after shot, *c* — the digital Excel view of the thermogram. The green color marks a target area (in the online version).

1 and converted to the digital form (an array of 160×120 dots). Fixing the thermograms and calculation of the energy density in each point were performed as per a procedure described in [11]. In order to obtain the full energy per the thermal imaging target (which was the collector) the average energy density was calculated in the marked area (Fig. 1,*c*) and multiplied by an area of this region ($95 \, \text{cm}^2$). Besides, the average density of the beam energy in its central part of the diameter of 4 cm was determined, which is important for selecting a mode of processing samples and/or parts. The thermal imaging target was a stainless steel foil of the thickness of 0.2 mm and the diameter of 11 cm, which is covered by the black frosted paint at the rear side, which provided the radiation coefficient of 0.95. The pause between the pulses was $4-5$ min, which was enough for cooldown of the target to the room temperature. The difference between the „hottest" and „coldest" point of the background thermogram (Fig. 1,*a*) does not exceed $1.5°\text{C}$, which is by one order less than the value of target heating within a beam autograph.

Due to the good pulse-to-pulse stability of the beam parameters, the vast majority of the experiments had a number of the series pulses limited to five (in order to increase the measurement accuracy at the charge voltage of $U_{ch} = 7 \, \text{kV}$, the thermogram was fixed after a package of the three consecutive pulses; at $U_{ch} = 10, 15$ and $20 \, \text{kV}$ the thermograms were fixed after one pulse).

The experimental diagram for recording the waveforms and thermograms in one pulse is shown in Fig. 2. A holder of the thermal imaging target was connected to the radial rod current conductor, thereby simultaneously recording the waveform of the beam current and its thermogram. It had improved the reliability and clarity of the comparative measurements of the beam energy in comparison with alternative measurement of the same magnitudes. Besides, this diagram also allows panoramically recording the distribution of the energy density across the beam cross section. The dissymmetry of the beam current output had not resulted in somewhat noticeable lateral beam

shifting: the induction of the external guide magnetic field of 0.11 T was enough for its retention.

2. Experimental results and discussion

The first cycle of the experiments was dedicated to measurement of the beam energy by the oscilloscope and thermal imaging methods depending on the charge voltage U_{ch} for the two types of the diode.

Typical waveforms of the pulses of the accelerating voltage, the full cathode current and the collector beam current are shown in Fig. 3.

Figure 4 shows the dependences of the beam energy values in the pulse as calculated by the waveforms (E_{bw}), calculated by the thermograms (E_{bt}), the efficiencies of transmission of HVPG-stored energy to the beam energy (E_{bt}/E_{st}), and of the average energy density (W_{bt}) in the central part of the beam of the diameter of 4 cm on U_{ch}. It is clear from the data presented that the value E_{bw} is $1.6-2.73$ times higher than the value E_{bt}, and this difference is significantly higher than the measurement error not exceeding $\pm10\%$ for the both methods of the beam energy measurement. This discrepancy can be explained by the fact that the beam current is overestimated due to contact of the collector with plasma emergent near its surface. This effect is known for quite a long time [12]. By the example of their beam ($200 \, \text{keV}, 250 \, \text{A}, 25 \, \text{A/cm}^2, 80 \, \mu\text{s}$), the authors [12] have demonstrated that decay of the collector plasma (the ions of this plasma go away radially to a drift tube wall, and the electrons go to the collector along force lines of the external magnetic field) substantially contributed to the beam current (but not to its energy as the plasma electron energies are close to the thermal one). The ion current to the drift tube occurred approximately in $40 \, \mu\text{s}$ after the start of the pulse and was 200 A at its peak, i.e. at this stage almost the entire collector current consisted of the decay plasma current. This ion current multiply exceeded the Child−Langmuir limit for the vacuum diode, but [12] gives no explanation to this fact.
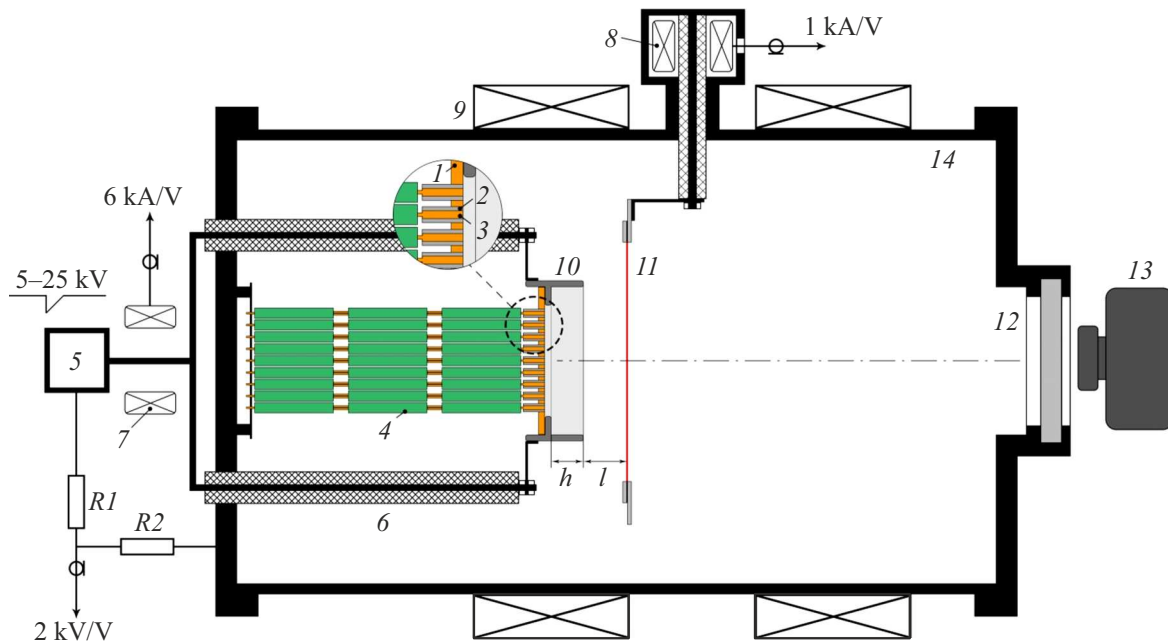
Figure 2. Experimental scheme with simultaneous recording of the beam current waveforms and its thermograms. *1* —cathode, *2* — ceramic tubes, *3* — copper electrodes, *4* — TVO-2 resistor (1 kΩ each), *5* — high-voltage pulse generator (HVPG), *6* — accelerating voltage inputs, *7* and *8* — the Rogowsky coils, *9* — solenoid, *10* — screen electrode with the height of $h = 15$ mm, *11* — thermal imaging target, *12* — calcium fluorite window, *13* — thermal imager, *14* — gun frame. *R1* and *R2* — resistive voltage divider.
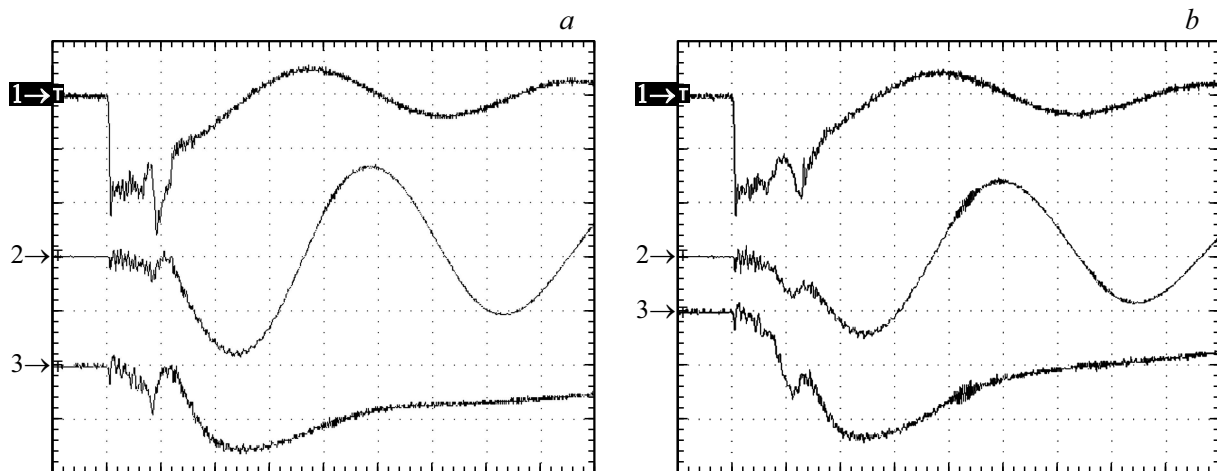
Figure 3. Typical waveforms of the accelerating voltage pulses (Ch1, 10 kV/div), the total cathode current (Ch2, 24 kA/div) and the collector beam current (Ch3, 10 kA/div); the horizontal scale — 1 μs/div. The HVPG charge voltage $U_{ch} = 15$ kV, $l = 20$ mm. *a* — the vacuum diode; *b* — the gas-filled diode. The argon pressure is $p = 0.093$ Pa.

The results similar in the nature thereof were obtained by the authors in the papers [13–15] on an electron source with a mesh plasma emitter „SOLO" (15 keV, 200 A, 10−15 A/cm², 100 μs). This source formed and transported the beam in a low-pressure gas (argon or helium, the pressure from 0.1 to 2 Pa) in a guide magnetic field to 30 mT. The transport channel length was dozens of centimeters. The gas was quite quickly (in several microseconds) ionized (the ionization degree was up to dozens of percent), thereby ensuring the high efficiency of the beam transport to the collector. The ion current to the drift tube was up to 50−80 A, while the energy measured by the calorimetric was 1.5 times less than the value obtained from the waveforms.

It is clear from the data of Fig. 4 that the efficiency of transmission of the stored energy to the beam energy E_{bt}/E_{st} falls with the increase in U_{ch}. It probably can be correlated to the increase in losses of the electron current both in the radial direction due to anomalous diffusion of the electrons out of the cathode plasma [8,16,17], and to drop

	Vacuum diode				Gas-filled diode ($p = 0.093$ Pa)			
E_{bt}/E_{st}, %	38.6	33.30	31.30	19.9	47.10	40.30	32.50	23.50
W_{bt}, J/cm^2	0.9	1.45	3.96	5.2	1.11	1.95	3.86	5.23
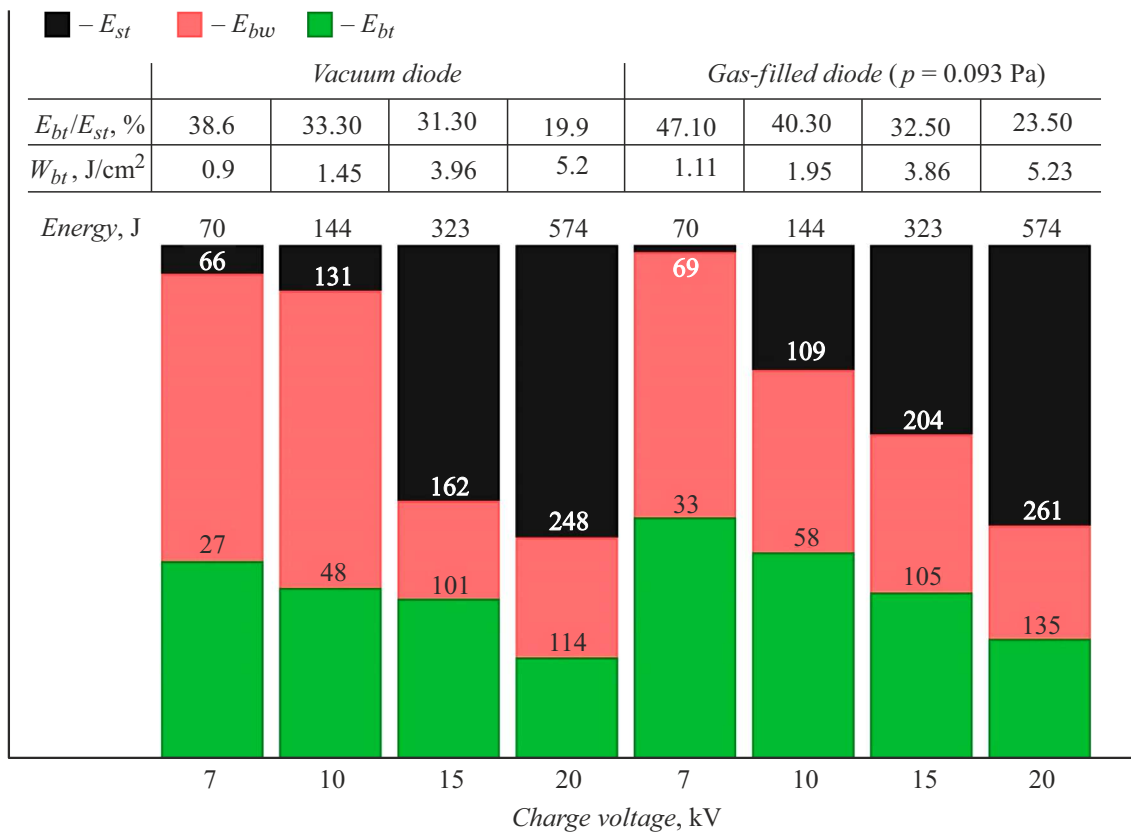
Figure 4. Diagrams of values of the beam energy for the two types of the diode, the efficiency of transmission of HVPG-stored energy to the beam energy and of the average energy density in the central part of the beam.

of the dielectric strength along the surface of the resistors of the cathode assembly. The latter had to be clarified in the future. Note also that the values E_{bt} and E_{bt}/E_{st} for the gas-filled diode are by $10-22\%$ higher than for the vacuum diode, which is caused, we think, by better match of the HVPG with the load. The energy density for the gas-filled diode is also higher for $U_{ch} = 7$ and 10 kV, and for $U_{ch} = 15$ and 20 kV it is almost the same as for the vacuum diode.

The beam energy densities at $U_{ch} = 15$ and 20 kV obtained for the traditional gun with the plasma anode and the multi-wire copper cathode [8], were compared with the present results to show that in the latter the energy density is higher by about $25-30\%$.

It is obvious that the beam energy in the pulse as determined from the thermograms is much closer to the true value. It is not only due to the fact that the physical cause of the overestimated beam current is understood, but also because the correctness of thermal imaging was repeatedly confirmed by calorimeter measurements and coincidence with the calculated [18,19] and experimental values of pulse melt thresholds of the metallic targets [8]. Actually, the thermal imaging measurements of the beam energy are essentially calorimetric measurements.

Note that the alternate measurements of the beam energy in the pulse have also shown that approximately twofold exceeding of the values obtained by the oscilloscope method

above the values obtained using the thermal imager. The high emissivity of the collector plasma can be confirmed by the following evaluations. Let us use the approximate formula (2.11) of [8] to determine the density of the charged particles of the collector plasma, which is formed from the desorbed gas:

$$n_{cp} = \left(\frac{j_e}{e}\right)^2 \frac{\gamma \sigma_i t}{\upsilon_g}. \tag{1}$$

Here j_e — the t-averaged density of the current of beam electrons bombarding the collector, e — the electron charge, γ — the coefficient of electron-stimulated desorption, σ_i — the cross section of ionization of the desorbed gas molecules by the beam electrons, υ_g — the rate of thermal expansion of the desorbed gas. It is clear from the formula (1) that the value n_{cp} has substantial values in case of the beams of the high current density and/or pulse duration. By inputting the typical values $j_e = 320$ A/cm^2, $\gamma = 3$ (see, for example, [20]), $\sigma_i = 5 \cdot 10^{-18}$ cm^2, $\upsilon_g = 10^5$ cm/s, $t = 10^{-6}$ s, into (1), we obtain $n_{cp} = 6 \cdot 10^{14}$ cm^{-3}. The corresponding density of the emission current of the electrons of this plasma will be 2400 A/cm^2 at the typical thermal speed of electrons 10^8 cm/s, so will the density of the emission ion current dozens of A/cm^2. It should be also noted that these values of plasma density and emission current are rather an assessment from below as it does not take into account
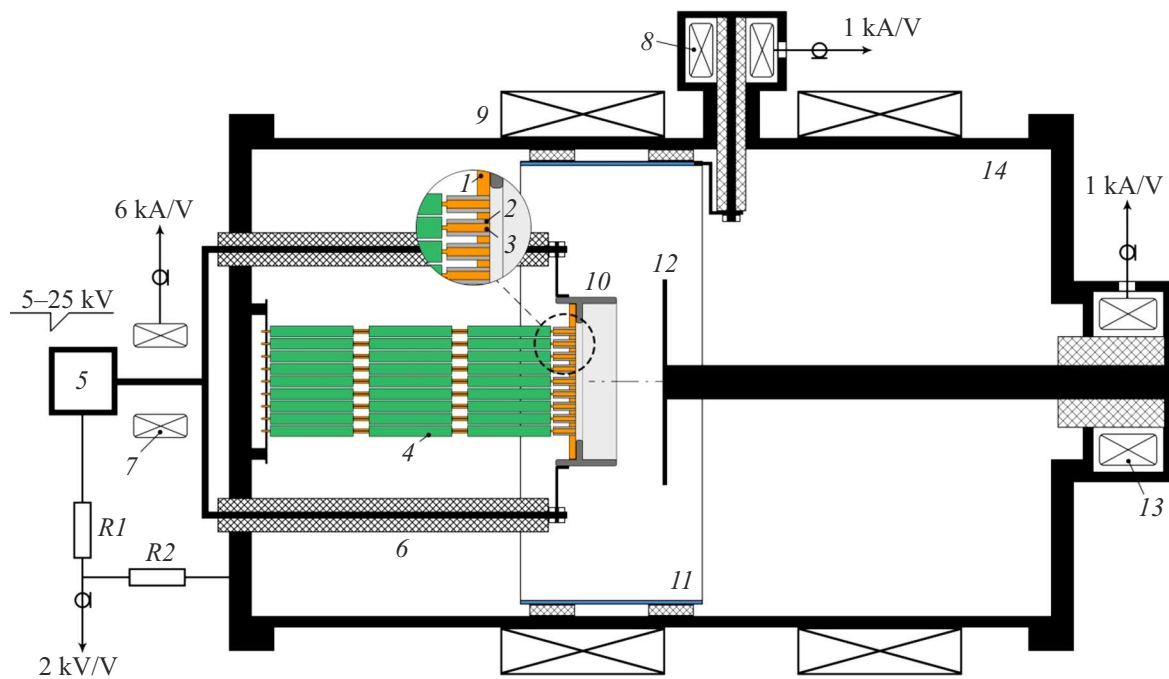
Figure 5. Experimental diagram for recording the ion current to the drift tube. *8* — the Rogowsky coil designed to measure wall collector beam current *11*, *12* — beam collector, *13* — the Rogowsky coil designed to measure collector beam current *12*. The rest is the same as in the caption of Fig. 2.
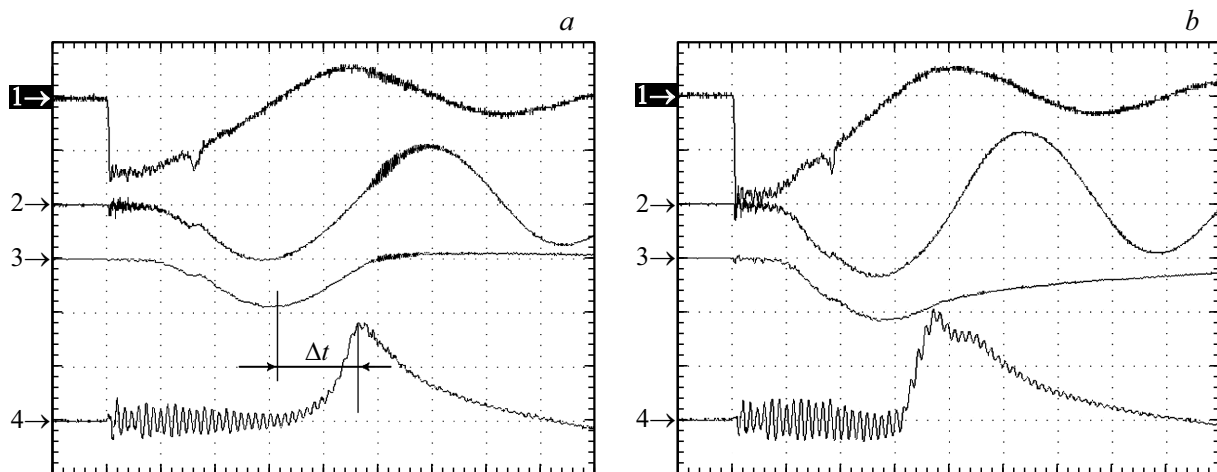
Figure 6. Typical oscillograms of the accelerating voltage pulses (Ch1, 10 kV/div), the total cathode current (Ch2, 24 kA/div), the collector beam current (Ch3, 25 kA/div) and the wall collector current (Ch4, 2 kA/div); the horizontal scale — 1 μs/div. $p = 0.093$ Pa, $l = 20$ mm, $U_{ch} = 10$ kV (*a*) and 15 kV (*b*).

ionization of the desorbed gas by the electrons generated in formation of the electron-ion pair, which can have the energies above the ionization potential [14,21]. The ionization of the desorbed gas can be additionally contributed also by beam electrons reflected from the collector and by the secondary electrons dislodged therefrom. At the above values, the rate of recombination reducing the density of charged particles is small, therefore, the recombination may be omitted in our evaluations. The density of the collector plasma can be mainly limited by a finite margin

of the adsorbed molecules, but it is sufficient for our beam current densities and duration of its pulse. Indeed, taking into account the surface roughness, there is approximately 10^{16} molecules in one monolayer per 1 cm^2 of the surface projection [22]. The molecule consumption for generation and removal of the charged particles for the pulse time τ_p will be $j_i \tau_p / e \approx 10 - 20 \, \text{A/cm}^2 \cdot 4 \cdot 10^{-6} \, \text{s} / 1.6 \cdot 10^{-19} \, \text{C} = (2.5 - 5) \cdot 10^{14}$ particles/cm^2. Thus, when there are 2−3 monolayers of the adsorbed gases on the collector surface, the margin of the molecules appears to be sufficient to

ensure the decay current of the collector plasma, which is determined exactly by ion removal [23]. With increase in the beam energy density, the density of the collector plasma will be increased due to evaporation of the collector material: for the beam of our duration it can play a substantial role at the energy density above $7-10\,\mathrm{J/cm^2}$ [18,19].

It is obvious that the decay plasma current reduces the energy efficiency of the electron source, as because of it the diode impedance reduces due to acceleration of the HVPG capacitive storage discharge, while the energy of the plasma electrons leaving to the collector is very small in comparison with the energy of the cathode-emitted electrons.

In order to confirm the availability of the decay current of the collector plasma, we have performed the experiment for recording the ion current to the drift tube. The experimental diagram is shown in Fig. 5, so are the typical waveforms in Fig. 6.

A large number of the waveforms has been studied to demonstrate that the range of the charge voltages $U_{ch} = 10-20\,\mathrm{kV}$ exhibited the wall collector current at the beginning of decay (in terms of an absolute value) of the cathode current and the collector beam current, whereas its value was quite unstable from pulse to pulse and was $1-4\,\mathrm{kA}$. At the charge voltage of $7\,\mathrm{kV}$, the wall collector current was not observed or was very small, which is probably correlated to substantial drop of the density of the collector plasma.

A part of the ion current was removed to the cathode. And we do not know the value of this part, but, assuming it is close to the Child-Langmuir limit for the bipolar flux, then it will be about 1% of the collector electron beam current. Thus, the ion currents observed at the wall collector only partially compensate the unbalance in the beam energy values determined by the thermal imaging and oscillograph methods.

Note that the radial flowing of anomalously large ion currents is difficult to explain since the length of the radial vacuum gap is above 7 cm. We suggest that the space charge of ions is almost entirely compensated by the electrons emitted by the cathode spots, which were generated at the edge of the screen electrode *10* (Fig. 2) due to the „capture" effect under the plasma of the arc sources [24]. The part of these electrons drifts simultaneously both azimuthally in the crossed $E_r \times B_z$ fields and axially. Thus, the space between the collector and the wall generates the layer of the negative space charge, which compensates the space charge of the ions. Probably, the part of these electrons hits the wall collector, thereby reducing the value of the positive signal. Naturally, the proposed pattern is of a hypothesis, which requires additional studies including the numerical modelling.

The kinetic ion energies can be evaluated by the delay time Δt (Fig. 6) between the beginning of the NHEB current fall and the moment of the maximum wall collector current. If assuming that the average speed of the ion of the M mass and the Z charge is equal to $\upsilon_i = (1/2)(2ZeU/M)^{1/2}$, then

the ion energy will be

$$ZeU = 2M\upsilon_i^2. \tag{2}$$

Assuming that $\upsilon_i = (r_{wc} - r_b)/\Delta t$, we obtain $\upsilon_i = (9.8 - 2.5)/1.4 \cdot 10^{-6} \approx 5.2 \cdot 10^6\,\mathrm{cm/s}$. Here, r_{wc} and r_b — the radii of the wall collector and the beam, respectively. By inputting this value into (2), we obtain that, for example, for the singly-ionized water molecule $ZeU \approx 1020\,\mathrm{eV}$, thereby approximately corresponding to the voltage drop of the collector inductor (about $90\,\mathrm{nH}$) and, therefore, to the potential difference between the beam collector and the wall collector. Naturally, the ion flux also contains other ions (from protons to oxygen ions), but studying their mass spectra and energy spectra is not included in the present paper.

It should be also noted that the positive signal observed at the wall collector can not be identified with the removal of the electrons therefrom. After several hundred pulses, the surface of this collector has been visually checked to show no trace of the cathode spots.

Conclusion

The energy characteristics of the high-current electron gun with the arc plasma sources built therein cathode assembly were investigated to show that the efficiency of transmission of the stored energy into the beam energy drops with the increase in the charge voltage of the high-voltage pulse generator powering the electron gun. For the gas-filled diode, the beam energy and the ratio of its value to the value of the generator-stored energy are higher by $10-22\%$ than for the case of the vacuum diode.

In order to determine the energy and the energy density of the intense electron beam in the pulse, the calorimeter (thermal imaging) measurements should be used. The oscilloscope measurements significantly overestimate (in our case up to 2.73 times) the beam energy due to the decay current of the collector plasma, whose ions in a considerable amount leave to the gun body wall. The current balance and the beam energy are to be quantitatively refined in further experiments as well as in thorough numerical modelling and calculations.

It is assumed that the high ion currents to the gun body wall are caused by generation of the negative space charge of electrons within the space between the collector and the layer wall, which compensates the space charge of the ions. The appearance of this layer is correlated to the azimuthal and axial drift of the electrons emitted form the edge of the cathode screen electrode.

application to solve scientific and technological problems", the project „Low-temperature plasma of stationary and pulsed discharges in gases and vacuum and its application in electrophysical devices" № FWRM-2021-0007.

Conflict of interest

References

[1] L.L. Meisner, V.P. Rotshtein, V.O. Semin, S.N. Meisner, A.B. Markov, E.V. Yakovlev, F.A. D'yachenko, A.A. Neiman, E.Yu. Gudimova. Surf. Coat. Technol., **404**, 12644 (2020). https://doi.org/10.1016/j.surfcoat.2020.126455

[2] S.N. Meisner, E.V. Yakovlev, V.O. Semin, L.L. Meisner, V.P. Rotshtein, A.A. Neiman, F. D'yachenko. Appl. Surf. Sci., **437**, 217 (2018). https://doi.org/10.1016/j.apsusc.2017.12.107

[3] Akira Okada, Yasuhiro Okamoto, Yoshiyuki Uno, Kensuke Uemura. J. Mater. Proces. Technol., **214**, 1740 (2014). http://dx.doi.org/10.1016/j.jmatprotec.2014.02.028

[4] J.W. Murray, J.C. Walker, A.T. Clare. Surf. Coat. Technol., **259**, 465 (2014). http://dx.doi.org/10.1016/j.surfcoat.2014.10.045

[5] Jie Cai, Qingfeng Guan, Xiuli Hou, Zhiping Wang, Jingxin Su, Zhiyong Han. Appl. Surf. Sci., **317**, 360 (2014). http://dx.doi.org/10.1016/j.apsusc.2014.08.049

[6] Yu. Ivanov, W. Matz, V. Rotshtein, R. Günzel, N. Shevchenko. Surf. Coat. Technol., **150**, 188 (2002).

[7] M.C. Li, S.Z. Hao, H. Wen, R.F. Huang. Appl. Surf. Sci., **303**, 350 (2014). http://dx.doi.org/10.1016/j.apsusc.2014.03.004

[8] G.E. Ozur, D.I. Proskurovsky. *Istochniki nizkoenergeticheskikh silnotochnykh elektronnykh puchkov s plazmennym anodom* (Nauka, Novosibirsk, 2018), ISBN 978-5-02-038794-2 (in Russian).

[9] P.P. Kiziridi, G.E. Ozur. Pis'ma v ZhTF, **46** (15), 47 (2020) (in Russian). DOI: 10.21883/TP.2022.06.54421.316-21 [P.P. Kiziridi, G.E. Ozur. Tech. Phys. Lett., **65** (2), 297 (2020). DOI: 10.1134/S1063784220020097]

[10] V.I. Petrov, P.P. Kiziridi, G.E. Ozur. ZhTF, **91** (11), 1764 (2021) (in Russian). DOI: 10.21883/JTF.2021.11.51541.80-21

[11] P.P. Kiziridi, A.B. Markov, G.E. Ozur, V.P. Frolova. Izv. vuzov. Fizika, **57** (3/2), 114 (2014) (in Russian).

[12] A.V. Lazarenko, E.S. Chebukov, V.I. Engel'ko. ZhTF, **59** (7), 159 (1989) (in Russian).

[13] S.V. Grigoriev, V.N. Devyatkov, N.N. Koval', P.V. Moskvin, A.D. Teresov. Trudy II Mezhdunar. Kreyndelevskogo seminara „Plazmennaya emissionnaya elektronika" (Ulan-Ude, 23−30 iyunya 2009), p. 30−36 (in Russian).

[14] S.V. Grigoriev, P.V. Moskvin, A.D. Teresov. Trudy IV Mezhdunar. Kreyndelevskogo seminara „Plazmennaya emissionnaya elektronika" (Ulan-Ude, 25−30 iyunya 2012), p. 112−117 (in Russian).

[15] N.N. Koval, S.V. Grigoriev, V.N. Devyatkov, A.D. Teresov, P.M. Shchanin. IEEE Transactions on Plasma Sci., **37** (10), 1890 (2009).

[16] M.V. Nezlin. *Dinamika puchkov v plazme* (Energoatomizdat, M., 1982) (in Russian).

[17] A.V. Gordeev. Fizika Plazmy, **32** (9), 847 (2006) (in Russian).

[18] V.P. Rotshtein, Yu.F. Ivanov, A.B. Markov, D.I. Proskurovsky, K.V. Karlik, K. Oskomov, B.V. Uglov, A.K. Kuleshov, M.V. Novitskaya, S. Dub, Y. Pauleau, I.A. Shulepov. Surf. Coat. Technol., **200**, 6378 (2006).

[19] A.B. Markov. Kand. dis. (Institut sil'notochnoi elektroniki, Tomsk, 2001) (in Russian).

[20] E.N. Abdullin, G.P. Bazhenov. ZhTF, **51** (9), 1969 (1981) (in Russian).

[21] G. Kal'man, B. Rozen. UFN, **12** (1), 105 (1932) (in Russian).

[22] Ya. Groshkovskiy. *Tekhnika vysokogo vakuuma* (Mir, M., 1975) (in Russian).

[23] B.G. Mendelev, L.A. Svyatochevskaya. ZhTF, **21** (1), 18 (1951) (in Russian).

[24] D.I. Proskurovsky, V.F. Puchkarev. ZhTF, **49** (12), 2611 (in Russian). (1979).